Blueprint Academic Publishers

Journal of Aquatic and Terrestrial Ecosystems
Journal ISSN: 2960-1118
3(3)
Received: September 14, 2025
Accepted: November 18, 2025
Published: December 12, 2025

Adsorption Isotherm, Kinetic and Thermodynamic Studies for The Removal of Rhodamine B and Heavy Metals (Co^{2+}, Cu^{2+} and Pb^{2+}) from Wastewater using Rice Husks, Coconut Shells and Clay

Gichuki G. John *, Okoth O. Maurice, Lutta T. Samwel and Lusweti K. John

Department of Chemistry & Biochemistry, School of Science, University of Eldoret, P.O. Box 1125-30100, Eldoret, Kenya

Abstract

The contamination of aquatic environments by heavy metals and synthetic dyes requires cost-effective and sustainable remediation strategies. This study evaluates the efficiency of powdered adsorbents derived from rice husks (ARC), coconut shells (ACC) and clay soil (ACS) for the removal of $Co^{2+,}$ Cu^{2+}, Pb^{2+}, and Rhodamine B (RB) dye. The adsorbents were characterized using XRD, XRF, FTIR, and BET analysis to determine their mineral phases, elemental composition, functional groups, and surface area. Metal concentrations were analyzed using Atomic Absorption Spectroscopy (AAS). Batch adsorption experiments were conducted to examine the effects of temperature, contact time, solution pH, and initial concentration dosage. For Co^{2+}, Cu^{2+}, Pb^{2+} ions, and RB, equilibrium and kinetic studies were conducted at 25 °C with particle sizes of 100 µm at optimal pH values of 4, 7, and 12. Thermodynamic assessments were also conducted, including variations in free energy, enthalpy, and entropy. The adsorption kinetics followed pseudo-second order kinetics, and the adsorption data fitted well the Langmuir isotherm model, with a correlation coefficient (R^2) > 0.99 for all adsorbates for the three adsorbents. Thermodynamic parameters revealed endothermic and non-spontaneous metal ion adsorption at low temperatures, however, with spontaneous adsorption at higher temperatures. High negative free energy change (ΔG^o) implies spontaneity, reflecting a more energetically favourable process driven by entropy. This study demonstrates carbonized biomass (rice husks, and coconut shells) and modified clay to be promising low-cost adsorbents for the removal of metal ions and dyes from aqueous solutions.

Keywords: Adsorbents, characterization, bioremediation, fabrication, Freundlich isotherm, biosorption, nutritional adoption

Correspondence: jmwg2005@yahoo.co.uk

Funding: The authors received no financial support for the research, authorship and/or publication of this article.

Data Availability Statement: The authors confirm that the data supporting the findings of this study are available within the article [and/or] its supplementary materials or upon reasonable request.

Competing interests: The authors declare no potential conflicts of interest with respect to the research, authorship and/or publication of this article.

Introduction

Recently, improper waste disposal has created major challenges for industrial activities in developed, emerging, and developing countries. As a result, even at low concentrations, these have led to the emergence of pollutants in water bodies that have serious health effects. It is difficult to treat wastewater from the food, paper, textile, and dyeing industries before releasing it into an aquatic environment due to high cost (Muiruri *et al.,* 2013). Toxic effluents from various industries negatively impact aquatic life, soil fertility, water resources, and the overall environment. One significant issue is the presence of colored wastewater from the textile sector. Brighter hues and a wide variety of colorants that are color-fast are available in synthetic dyes (Kant, 2012).

Light and informal (jua kali) businesses such as those that produce textiles, leather and paper goods, plastics, cement, metal working, wood preservatives, paints and pigments, and steel fabrication have experienced a notable surge in growth. These industries discharge large quantities of poisonous waste to water making it unhealthy for domestic use. Studies in Kenya have shown that open-air mechanical workshops are significant sources of mobile and bioavailable heavy metal contaminants (Chengo *et al.*, 2013). Several studies suggest that among the heavy metals, pollution associated with lead ions is of key concern (Muiruri *et al.,* 2013). Lead is a non-essential element and is toxic even at very low concentration resulting in impairment of nervous system (Tong *et al*., 2000). People have reported nausea and vomiting at a level of 15 mg/L of lead, with no negative impacts at 0.05 mg/L (Levin *et al*., 2008). Copper has a detrimental effect on nutritional adoption; it is a common component of many agricultural products and enters the food chain where it may pose a risk to human and animal health. Copper is a vital micronutrient for crops and can easily accumulate in surface waters. Consuming more copper than is advised can lead to serious liver and gastrointestinal problems (Kudesia, 2000).

There are a number of analytical techniques that can be employed to extract heavy metals from aqueous solutions. According to Banerjee *et al*. (2016), these processes include adsorption, chemical precipitation, ion exchange, ultra-filtration, reverse osmosis, and electrodialysis. These approaches have certain limitations because of their intrinsic operational issues. Adsorption has proven to be a more cost-effective method for removing metals from aqueous solutions than the previously stated approaches. Agricultural

waste and clay can serve as effective adsorbents for removal of metals and dyes from aqueous solution. Rice husks and coconut husks are termed as agricultural wastes and are usually thrown away after processing. The disposal of green coconut is not quantifiable, and generally occurs in inappropriate environments such as beaches and vacant lots, and it is therefore associated with the pollution of public spaces, as coconut shells can take up to ten years to degrade in the environment, causing unsightliness in the urban environment, as well as developing into breeding grounds for mosquitoes and spreading disease. Tayeh *et al.* (2021) state that because of the tiny grain size of rice husk, improper handling during combustion may result in air pollution. When disposed of wrongly, rice husks have significant environmental impacts, for example, burning which is a common practice, leads to toxic smoke emissions, harming air quality and exceeding quality standards for parameters like SO_2, CO and NO_2 (Hawali *et al.,* 2023). This study aimed to evaluate the efficiency of rice husks, coconut shells, and clay in removing RhB, Co^{2+}, Cu^{2+}, and Pb^{2+} through a comparative analysis of their adsorption isotherms, kinetics, and thermodynamics.

Materials and Methods

Every chemical used was analytical grade (provided by Sigma-Aldrich, UK; reagents ≥ 98.5 %).

Preparation of the adsorbents

Preparation of Coconut Shell and Rice Husk Charcoal

After gathering these materials, they were sun dried and then coconut shells were broken using a jaw crusher and then carbonized in a furnace under limited oxygen supply, at varying temperature profiles (from 600 to 1000 ^{0}C) in a furnace for two hours. They were allowed to cool, before being rinsed with distilled water to remove impurities and fine dust and then dried in an oven at 100 ^{0}C until a constant weight was achieved, before cooling again in a desiccator. Both coconut and rice charcoal materials were separately crushed and thereafter underwent particle size grading and screening before sorting for final applications using mesh sizes 18, 20 and 60. This unwashed form of charcoal was stored in a sealed glass container until use.

Washed coconut and rice charcoal were processed by using deionized water to wash until the pH of the effluent was < pH 8. This removes residual ash and soluble salts that could interfere with the adsorption sites. It was then dried overnight in an oven at 100 ^{0}C and stored in sealed glass containers until use.

Preparation of Clay

The unmodified bentonite clay was sourced from Isinya area, Kenya. To increase the functional group concentration, the bentonite clay was treated with 1 M hydrochloric acid (HCl), sulfuric acid (H_2SO_4) and sodium hydroxide (NaOH) in the ratio of 1 g clay to 50 mL solution separately to prepare different batches with different ranges of pH. The mixture was then shaken at speed of 120 rpm for 24 hours using an electrical shaker, and then washed with distilled water until a pH of about 6–7 was obtained. The modified clay then was separated from water by vacuum filtration and dried at room temperature, after that it was milled and sieved to obtain the average size of 0.074 mm in powder form. The modified and unmodified clays were then characterized for their porous properties.

Adsorbent Characterization

Using Empyrean, PANalytical X-ray diffractometer with CuKα radiation, the

crystalline structures of coconut shell and rice husk charcoal and clay were ascertained using X-ray diffraction (XRD) analysis. The diffraction patterns were obtained between diffraction angles of 0^0 and 90^0. Fourier transform infrared (FTIR) spectroscopy was used to identify the functional groups that could have an impact on the adsorption process (a PerkinElmer 2000 FTIR spectrometer). Plotting the volume adsorbed (cm^3/g STP) against relative pressure (P/Po) revealed the BET surface area, average pore volume, and size distribution of the raw adsorbent. The adsorbents' chemical makeup was ascertained through the application of XRF analysis technology. The Empyrean, PANalytical XRF spectrometer with 60 kV energy of the X-ray tube was used to evaluate all samples.

Metal Solution

All of the materials used in this experiment were of analytical grade. Lead stock solutions (1000 mg/L) were made by dissolving 1.60 grams of $Pb(NO_3)_2$) in distilled water in a 1000 mL volumetric flask. 4.93 grams of $Co(NO_3)_2.6H_2O$ were dissolved in 1000 mL of distilled water to prepare the cobalt ions stock solution. 3.76 grams of $Cu(NO_3)_2.3H_2O$ were dissolved in distilled water to make a stock solution of copper, 1000 mg/L. The solutions were then topped off with 1000 mL of distilled water. Working solutions were made by serially diluting stock solutions with distilled water to achieve the proper dilutions.

Adsorption Experiments

On dried coconut shells, rice husk charcoal, and clay, batch adsorption procedures were used by adjusting contact time, solution pH, adsorbent dosage, and temperature. In order to reach the equilibrium time, adsorption studies were performed by adding 1.0 g of the adsorbent to 50 mL of aqueous metal solutions containing 1 ppm Co^{2+}, Cu^{2+}, and Pb^{2+} ions in solutions, respectively, and RB dye in conical flasks set on a shaker. The study examined the impact of varying solution pH (2–12), adsorbent dosage (1, 2 and 5 g), contact time (30, 60, 90, 120, 150 and 180 minutes) and solution temperature (273–373 K) on the efficacy of metal ion and dye removal. The metal ion and dye concentrations were analyzed following filtration using Whatman 42 filter paper.

The percentage of dye removed at a given temperature, initial dye concentration, initial pH, adsorbent dose, ionic strength (when salts are added) and the duration of contact, was calculated in each case using the equation below:

$$\% \text{ removal} = ((C_i - C_e) / C_i) \times 100$$

where C_i and C_e (mg / dm^3) are the initial and equilibrium concentrations of the dye, respectively. The experiments were conducted in duplicate and the negative controls (with no sorbent) were simultaneously carried out to ensure that sorption was by the adsorbent material and not by the container.

Adsorption Isotherms

Adsorption isotherms were investigated using 5 g of the raw adsorbent added to 100 cm^3 of the appropriate multi-component solution and shaken for equilibrium time at 150 rpm. The agitation speed of 150 rpm was used for 120 minutes. The particle size of the adsorbents used was 60 µm. Two isotherm models, namely Freundlich and Langmuir, were employed.

Adsorption Kinetics

At the appropriate contact times, 5 g of each adsorbent was combined with about 50 cm^3 of each aqueous solution and thoroughly shaken. The mixture was kept at room temperature. First- and second order pseudo-adsorption kinetics

were computed using the acquired residual metal ion and dye concentrations.

Adsorption Thermodynamics

The temperature changes were used to compute the adsorption thermodynamic parameters while maintaining the initial concentration and weight of the adsorbent constant.

Results and Discussion

Characterization of the Adsorbent

To determine the functional groups in the adsorbents and the groups involved in metal ion binding, FTIR analysis was performed. Molecular substances were recognized by the analysis. This was accomplished by determining how much infrared radiation a sample could absorb. The compound's functional groups could then be determined by analyzing the resulting spectrum.

The FTIR spectra of ARC, ACC and ACS displayed a number of absorption peaks, which showed the complex nature of the adsorbent. The characteristic peaks at 3218 cm^{-1}, 3017 cm^{-1} and 3380 cm^{-1} indicated the presence of -OH groups of silanols (Si-OH) and siloxanes (Si-O-Si-OH), a fact that is confirmed by the intense absorption in 1058 cm^{-1}, 1020 cm^{-1}, and 990 cm^{-1}, respectively which showed a Si-O asymmetry stretching. This agreed with observations made by Vieira *et al.,* (2013). Vibrational peaks at 2460 cm^{-1}, 2424 cm^{-1} and 2446 cm^{-1} were for asymmetric stretching vibrations of O=C=O. The peaks at 795 cm^{-1}, 756 cm^{-1} and 778 cm^{-1} were due to vibrations of symmetrical stretching Si-H. The C=C stretching vibrations at 1600 cm^{-1}, 1557 cm^{-1} and 1625 cm^{-1} indicated the presence of alkenes and aromatic functional groups. The peaks at around 2924 cm^{-1} corresponded to C-H stretching vibration as reported by Bakti and Gareso (2018). The peaks indicated the complex nature of adsorbent and their capabilities of adsorption of heavy metal ions (Khan *et al.*, 2017).

FTIR spectrum in **Figure 1** displays peaks of different functional groups attributable to the adsorption of Cu^{2+} ions on ARC.

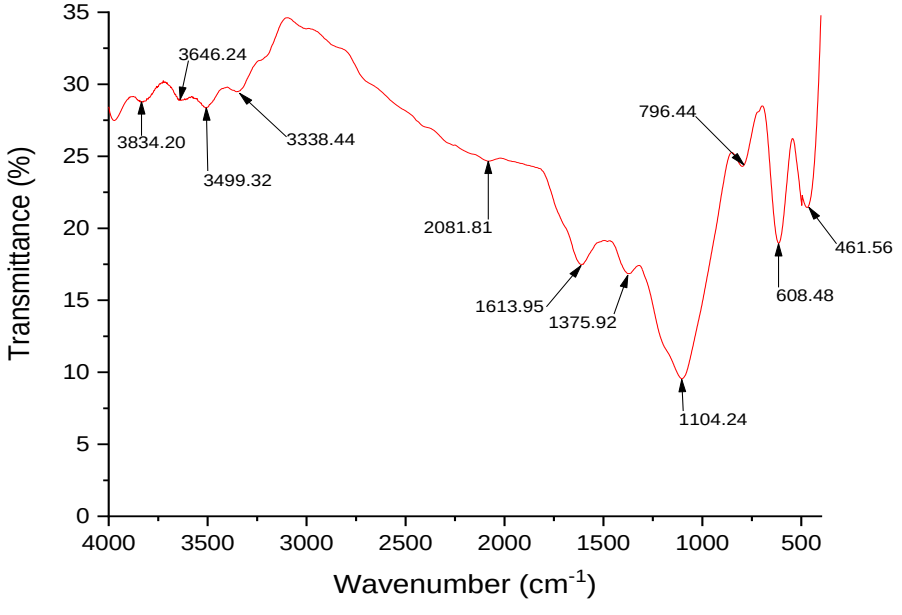

Figure 1: FTIR spectrum of ARC with copper

XRD patterns of the adsorbents of rice, coconut and clay revealed that rice and coconut activated charcoals are amorphous while clay is crystalline. The amorphism observed is explained by the rupture of multiple bonds C-C (mainly those of the aromatic rings) and the formations of the groups and functions on the surface during the preparation. These results also imply that all the samples have poor crystallinity making it a good adsorbent as higher crystallinity will lower the porosity and hence the surface area, and should lead to a "cleaner" surface, with less moieties and less defects, which are known to be energetic sites that are mostly utilized for adsorption (Zhao and Lang, 2018).

The XRF spectrometer was used to analyze the elemental composition of adsorbents. It was conducted to ascertain the elemental composition of each of the three adsorbents. The results for ARC, ACC and ACS are presented in **Table 1**. These results show that SiO_2, Al_2O_3, and K_2O are the main components, SiO_2 being dominant especially in ARC and ACS.

Table 1: Chemical composition (wt.%) for the adsorbents

	MgO	AL_2O_3	SiO_2	P_2O_5	S	Cl	K_2O	CaO	Ti	Cu	Co	Pb
ACC	0.00	2.11	4.30	5.76	2.31	3.58	65.48	11.04	1.21	0.00	0.00	0.00
ARC	0.00	0.34	94.26	0.78	0.13	0.05	2.00	1.55	0.09	0.00	0.00	0.00
ACS	6.07	14.14	63.90	0.02	0.31	0.03	6.45	2.17	0.56	0.00	0.00	0.00

The results indicate that SiO_2 and K_2O are the dominant oxides in the ARC, ACC and ACS at 94.261%, 4.306% and 63.895%, respectively for SiO_2 and 1.962%, 65.487% and 6.446% K_2O. Al_2O_3 in ACS was also high at 14.14%. The relatively high content of volatile inorganic and organic compounds, including carbon content, can be inferred from the loss on ignition, which indicates the content of volatile components of rice husk (Hegazi, 2013). Among the non-volatile components, silica was the most important.

Of interest is that cobalt, copper and lead were not detected in the three adsorbents. This was necessary to confirm so that they do not interfere with the experiment.

The nitrogen adsorption–desorption isotherms of the ARC, ACC and ACS adsorbents produced at 90 °C are shown in **Figures 2** to **4**. The type II and IV isotherm are seen.

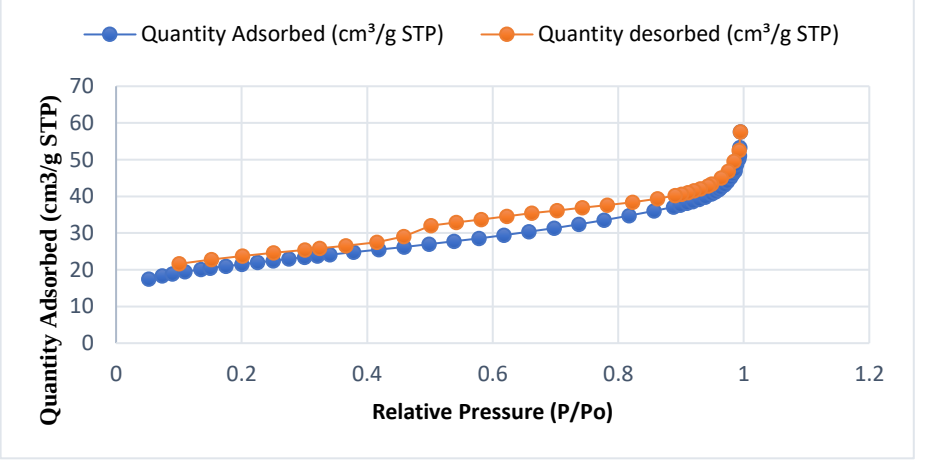

Figure 2: Adsorption isotherm of activated ARC

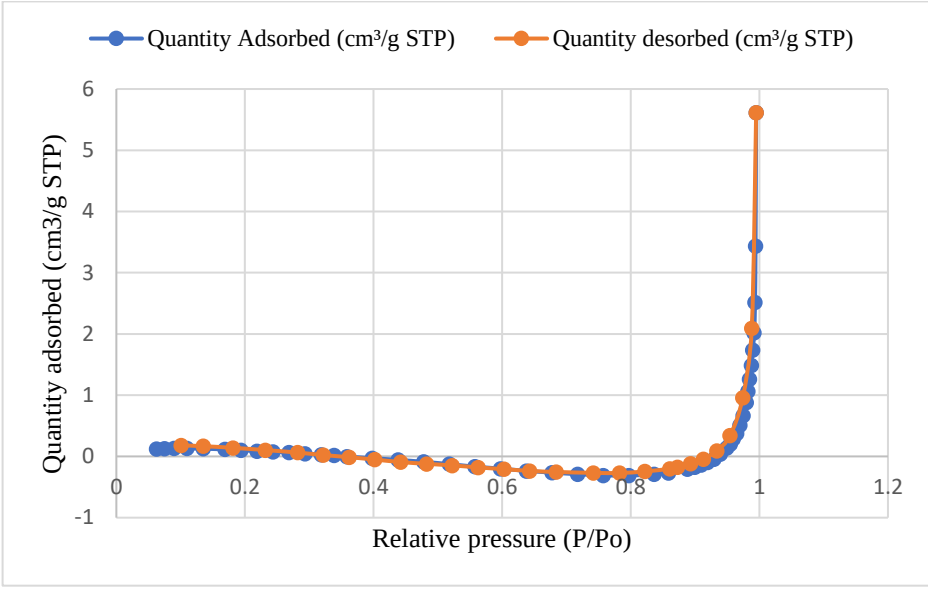

Figure 3: Adsorption isotherm of activated ACS

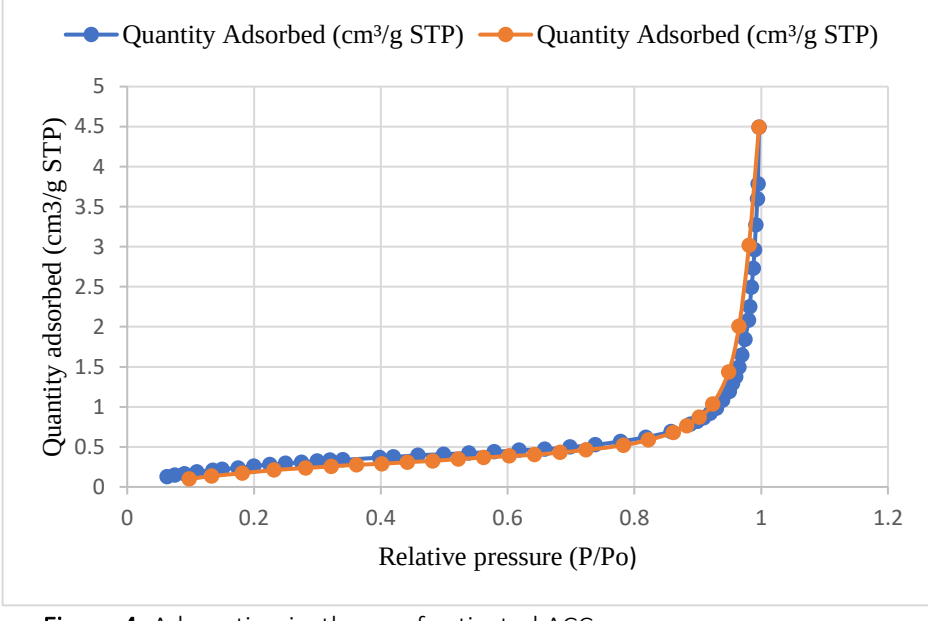

Figure 4: Adsorption isotherm of activated ACC

Srivastava *et al*. (2017) stated that the basis of BET analysis is the idea that, on a homogeneous surface, the rate of adsorption is equal to the rate of desorption. The results of this study demonstrated comparatively similar adsorption-desorption efficiency. This indicated the adsorbents were highly reusable and they have good stability. This could be attributed to their porous structure particles which enhanced adsorbent stability towards the elimination of metal ions and dye from aqueous solution. This attribute makes these adsorbents to be economically viable and proves their suitability as adsorbents for the treatment of wastewater. The extent of adsorption depends on the surface area of the solid. The determined pore volume and specific area are shown in **Table** 2.

Table 2: The BET surface area, micropore area, micropore volume and external surface area

Adsorbent	BET surface area (m^2/g)	Micropore area (m^2/g)	Micropore volume (cm^3/g)	External surface area (m^2/g)
ARC	72.0123	28.6609	0.008667	43.3515
ACC	1.1818	1.7029	0.000551	1.7029
ACS	0.2577	0.5300	0.000143	0.5300

The Effect of pH on Cu^{2+}, Co^{2+} and Pb^{2+} ions and RB Percentage Removal

The adsorption capacity decreased as the acidity of the contact solution increased. These variations can be explained by the competition between metal ions and hydrogen ions and by the variation of hydrolysis products of metal ions with pH (Wang *et al.*, 2007). The binding of various metal ions to biomaterials with distinct functional groups in competitive systems is contingent upon the ionic characteristics of these metals, including their electronegativity, ionic radius, potential, and redox potential (Naja *et al.,* 2010). The competitive selective adsorption between ions is related to the hydration radius and electronegativity of heavy metals (Pang *et al.,* 2018). From **Figures 5** to **7**, it was noted that cobalt was the most adsorbed followed by copper and lead the least. The assertion that larger ionic particles are less adsorbed than smaller ones is supported by this as well. The radius of hydrated metal ions affects adsorption selectivity, whereby the smaller the radius of hydrated metal ions, the less they are adsorbed by the adsorbent. Thus, Co^{2+} was more dominant in competitive adsorption. The hydration radius of Cu^{2+} (4.3 Å) is smaller than that of Co^{2+} (4.4 Å) and Pb^{2+} (4.5 Å) whereas the electronegativity of Pb^{2+} is lower (1.87 Å) than that of Cu^{2+} (1.9 Å) and Co^{2+} (1.23 Å) (Zhao *et al.*, 2019). The effect of initial solution pH on the adsorption of RB onto ARC, ACC and ACS is shown in **Figures 5 to 7**. The maximum equilibrium sorption capacity was obtained at pH 4 (75 %, 84 % and 90 % for ACS, ACC and ARC, respectively). In comparing the three adsorbents, ARC had the highest adsorbent capability followed by ACC and finally ACS. This could be explained in terms of surface area, pore size and pore volume. ARC possessed the highest surface area and high adsorption capacity as compared to ACC and ACS. This is well confirmed in the BET analysis in **Table 2**.

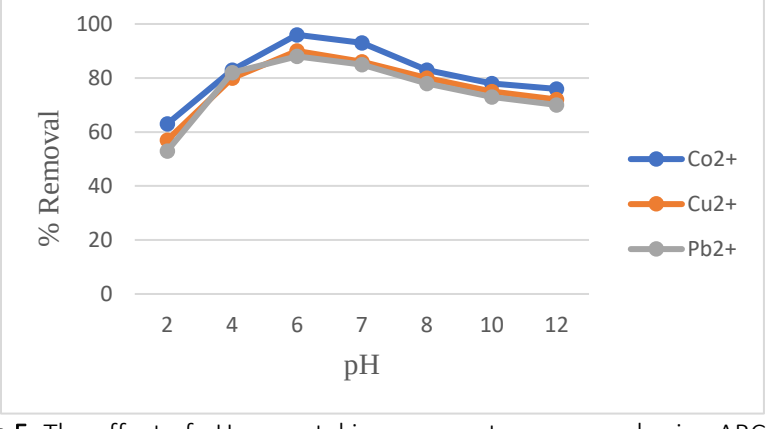

Figure 5: The effect of pH on metal ions percentage removal using ARC

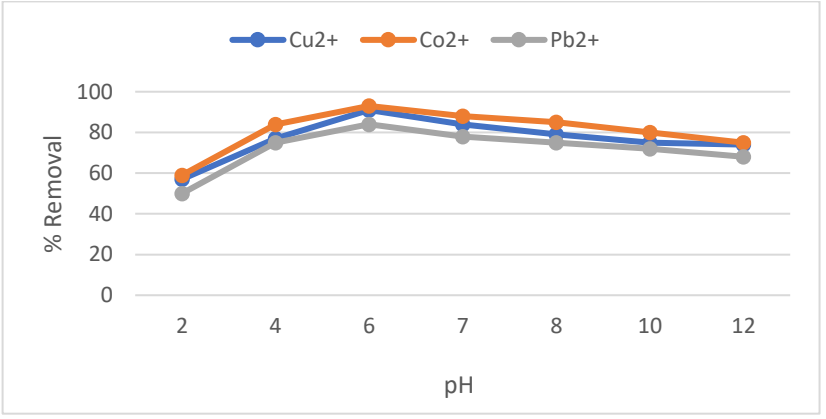

Figure 6: The effect of pH on metal ions percentage removal using ACC.

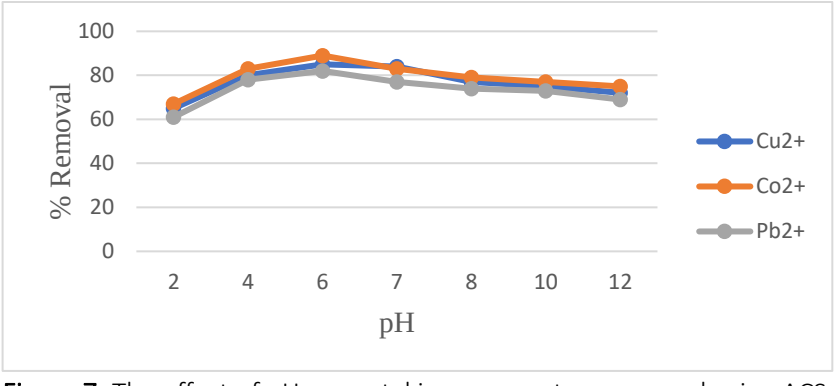

Figure 7: The effect of pH on metal ions percentage removal using ACS.

The effect of temperature on Cu^{2+}, $Co^{2+}$and Pb^{2+} ions and RB percentage removal

By changing the chemical interaction and the adsorbate's solubility, temperature has an impact on the adsorption rate (Singh *et al.,* 2001). The temperature of the solution rose from 273 to 373 K, increasing the amount of adsorbate adsorbed per unit mass of adsorbent. This increase illustrates the adsorption process' nature. The result shows that when the temperature rises, RB dye molecules are more mobile on an adsorbent. The temperature impact about the adsorption of Rhodamine B is shown in **Figure 8**.

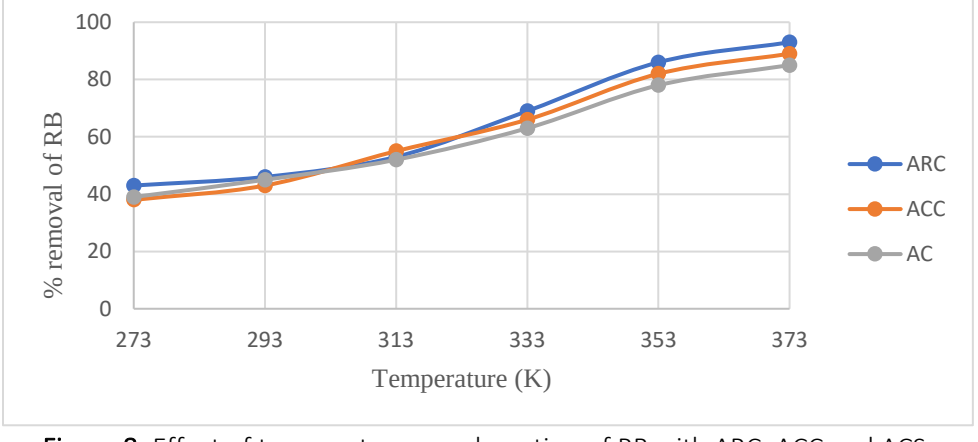

Figure 8: Effect of temperature on adsorption of RB with ARC, ACC and ACS

Increasing solution temperature leads to increased mobility of the dye molecules and thus enhances mass transfer of dye molecules from its liquid to solid phase of sorbent (Salleh *et al.*, 2011). Maximum adsorption rate regarding the three metal ions within the three adsorbates was found to be between 333 K and 353 K because the increase in temperature favoured the adsorption equilibrium. The three metal's process of adsorption indicated to be endothermic in nature. This is because the surface particles on adsorbents' surfaces were unstable and when the metal ions were adsorbed, the energy of the adsorbents increased resulting in the absorption of heat. Similar results were observed by Manyangadze *et al.,* (2020). **Figures 9** to **11** give comparison of the adsorption of metal ions on the three adsorbents.

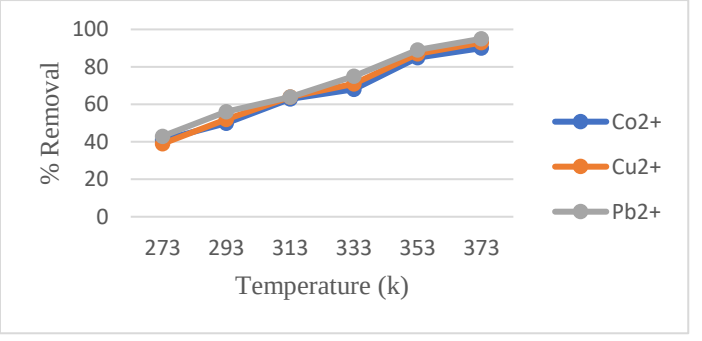

Figure 9: Effect of temperature on metal ions percentage removal using ARC

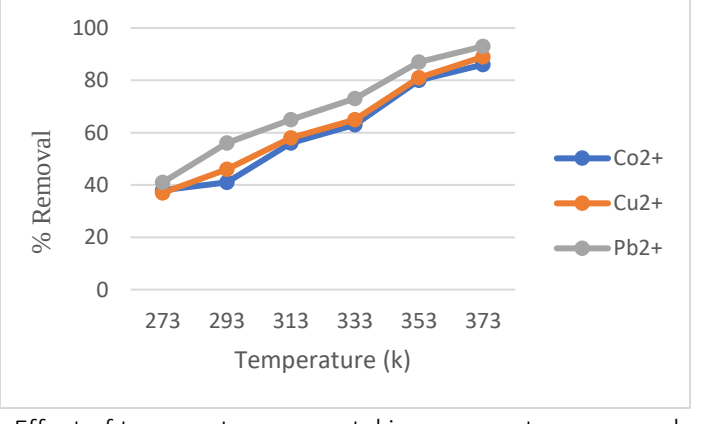

Figure 10: Effect of temperature on metal ions percentage removal using ACC

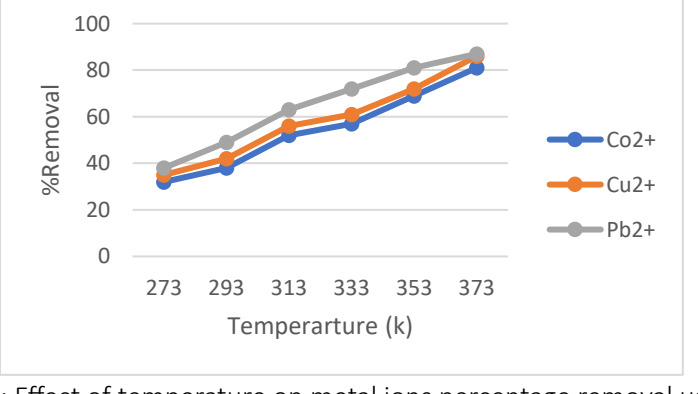

Figure 11: Effect of temperature on metal ions percentage removal using ACS

In all the adsorbents studied, Pb^{2+} ions were the most adsorbed especially in ARC with a 95 % as compared to Co^{2+} and Cu^{2+} with 90 % and 93 %, in ARC, respectively as indicated in **Table 3**.

Table 3: Effect of temperature on metal ions percentage removal using ARC

Temp (k)	Co^{2+}	Cu^{2+}	Pb^{2+}
273	41	39	43
293	50	52	56
313	63	64	64
333	68	71	75
353	85	87	89
373	90	93	95

The patterns demonstrate how rising temperatures increases ionic kinetic energies and provides more sorption sites in adsorbents, enhancing their adsorption capabilities. However, the electrostatic force of attraction between the adsorbate and binding sites reduces at temperatures above 353 K, favouring a slower rate of desorption and a reduction in the removal of ions (Mataka *et al*., 2010).

Effect of Shaking Speed on Cu^{2+}, $Co^{2+}$and Pb^{2+} ions and RB percentage Removal

Once the rate of shaking was over 100 rpm, the rates of removal of the dye rose as the shaking speed increased and reached a peak at 200 rpm, then the adsorption capacity of rhodamine B increased slightly with increasing shaking speed. For this reason, in the pertinent trials, a set shaking speed of 200 rpm was used. ARC turned out to be the superior adsorbent throughout the range of speeds. This is well illustrated in Figure 12 below.

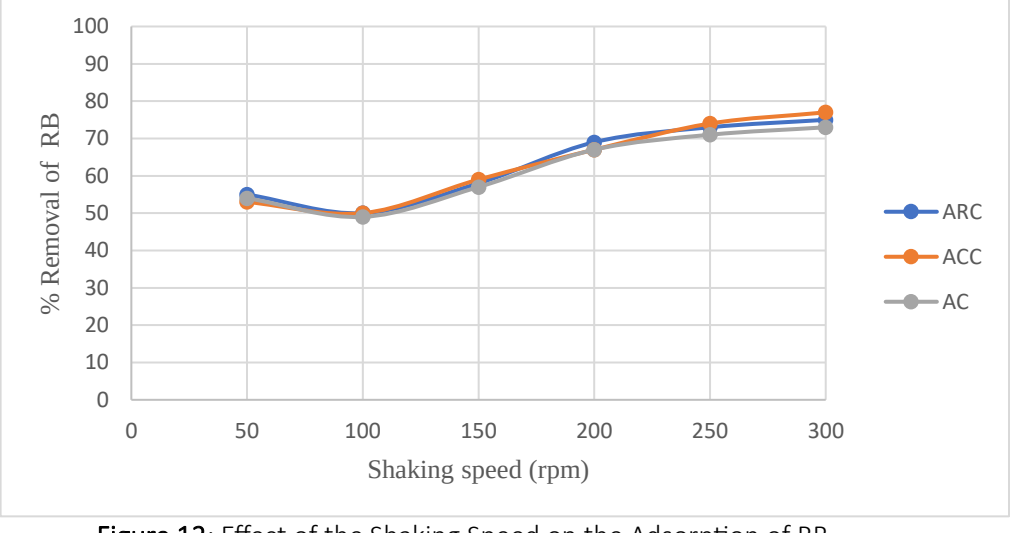

Figure 12: Effect of the Shaking Speed on the Adsorption of RB

Adsorption resulted in high selectivity for Co^{2+} over all the other available ions, thus $Co^{2+} > Cu^{2+} > Pb^{2+}$, with all the adsorbents used having above 80% removal efficiency at the speed between 200 and 250 rounds per minute as shown in **Figures 13** to **15**. This improvement in Co^{2+} adsorption could be due to its higher ionic potential and reduced size, which may result in a faster diffusion and stronger adsorption as an outcome of the acidic groups located at the pore edges. Therefore, smaller ion repels and hinders other ions from accessing the activated carbon pores (Irannajad and Haghighi, 2017).

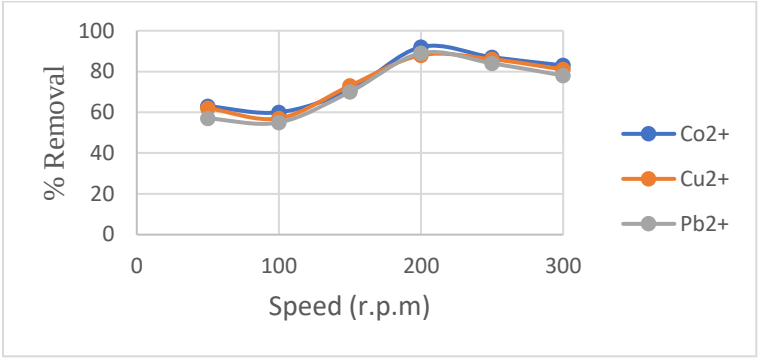

Figure 13: Effect of the shaking Speed on the Adsorption of metal ions in ARC

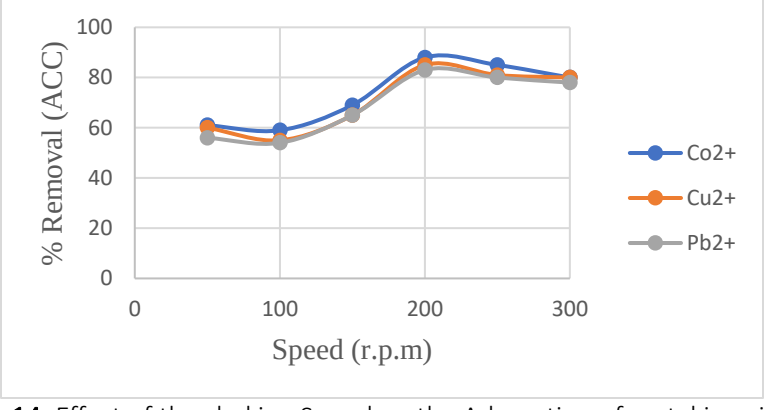

Figure 14: Effect of the shaking Speed on the Adsorption of metal ions in ACC

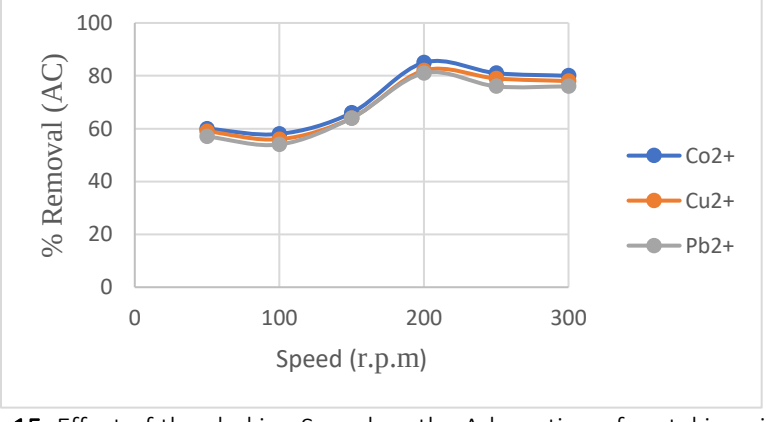

Figure 15: Effect of the shaking Speed on the Adsorption of metal ions in ACS

Therefore, from Figures 13 to 15, order of adsorbents' metal adsorption is: ARC >ACC >ACS.

Effects of contact time on Cu^{2+}, $Co^{2+}$and Pb^{2+} ions and RB percentage Removal

Impact of contact duration on the elimination of the dye Rhodamine B is illustrated in **Figure 16**. It demonstrates that the elimination of the dye increased with contact time and it was rapid initially up to 40 minutes, then proceeded at slower rate and finally almost attained saturation. This behaviour implies the adsorbent rapidly adsorbed on its exterior surface during the first stage, which may have been the rate-determining phase, then followed by a slower interior diffusion process.

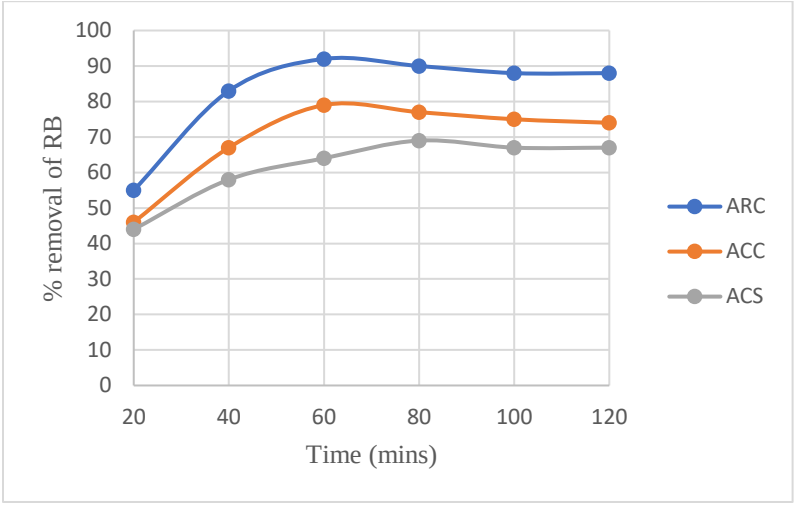

Figure 16: Effect of contact time on adsorption of RB with ARC, ACC and ACS

Figures 17 to 19 show how the length of contact time affects the adsorbents' capacity to absorb Pb^{2+}, Cu^{2+}, and Co^{2+} ions. To do this, the contact period was changed from 20 to 120 minutes in several experimental runs.

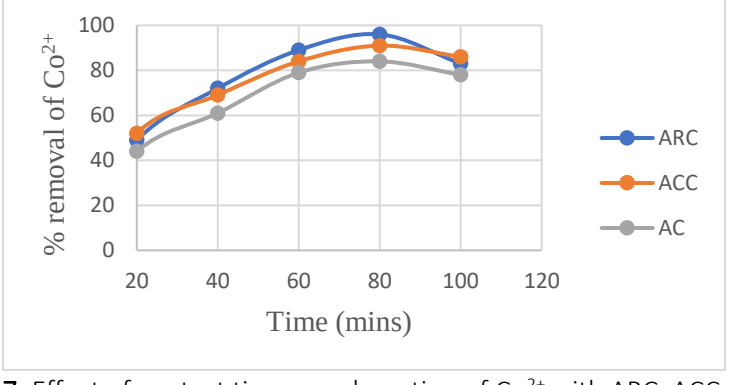

Figure 17: Effect of contact time on adsorption of Co^{2+} with ARC, ACC and ACS

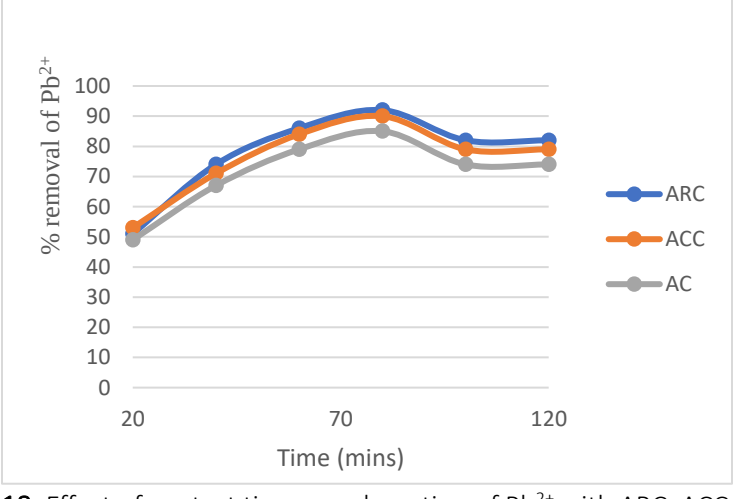

Figure 18: Effect of contact time on adsorption of Pb^{2+} with ARC, ACC and ACS

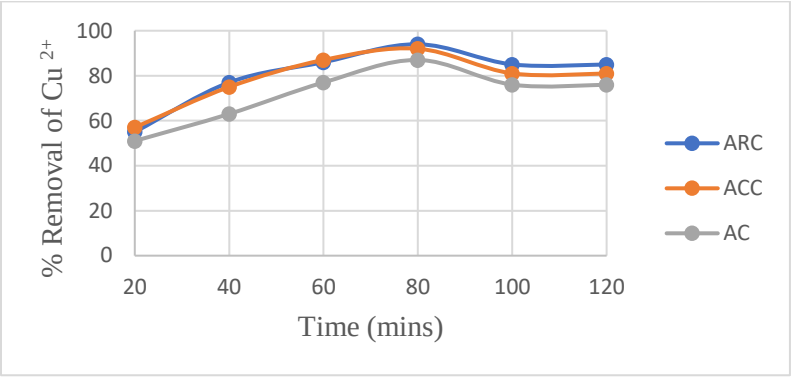

Figure 19: Effect of contact time on adsorption of Cu^{2+} with ARC, ACC and AC

Adsorption Isotherms

Equilibrium experiments were carried out using adsorbent masses of 5 g. The adsorbents were mixed with 100 mL solution of the appropriate multi-component solution. The agitation speed of 150 rpm was used for 120 minutes. The particle size of the adsorbents used was 60 µm. The linear form of Langmuir sorption isotherm is shown in equation below;

$$C_e/q_e = 1/K_{Lqmax} + 1/q_{max\ cvb}$$

where q_e is the adsorption capacity at equilibrium, q_{max} is the optimal adsorption of the adsorbent when the surface is fully saturated by the adsorbate, and C_e is the equilibrium concentration of the metal ions in milligrams per litre. The constant K_L is called the Langmuir constant and is indicative of the direction of the reaction. In the Langmuir adsorption isotherm, the separation factor is commonly denoted by the acronym R_L and is called the dimensionless separation factor or equilibrium parameter. It is calculated as:

$R_L = 1 / (1+K_L C_0)$

Where;

R_L = separation factor (dimensionless)

K_L= Langmuir constant (L/mg or related units), related to adsorption affinity

C_0 = initial adsorbate concentration (mg/L)

Adsorption of linearized Langmuir isotherms for adsorption of Co^{2+}, Cu^{2+} and Pb^{2+} ions and RB dye in ARC plotted as C_e/q_e against C_e are given in **Figures 20** to **22** and **Table 4**. From the figures, straight lines where 1/qmax and K_L were obtained from slopes and intercepts, respectively. All their K_L values were between 0 and 1, implying the reactions were favourable. Their corresponding R^2 values were 0.9935, 0.9986, 0.9976, and 0.9983 showing copper was the most adsorbed. This could be attributed to its small size and high charge which enabled it fit well to the available binding sites as observed by Nakbanpote *et al*., (2007).

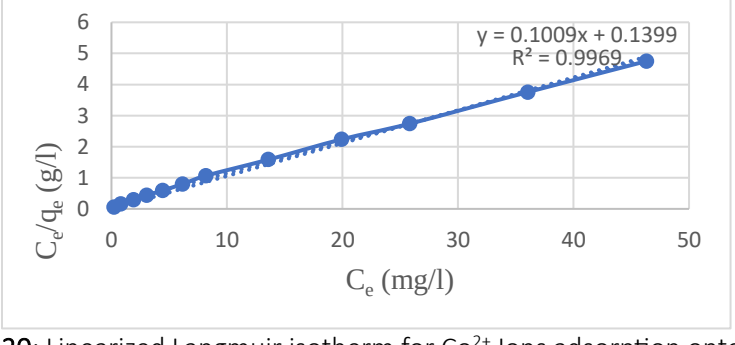

Figure 20: Linearized Langmuir isotherm for Co^{2+} Ions adsorption onto ARC

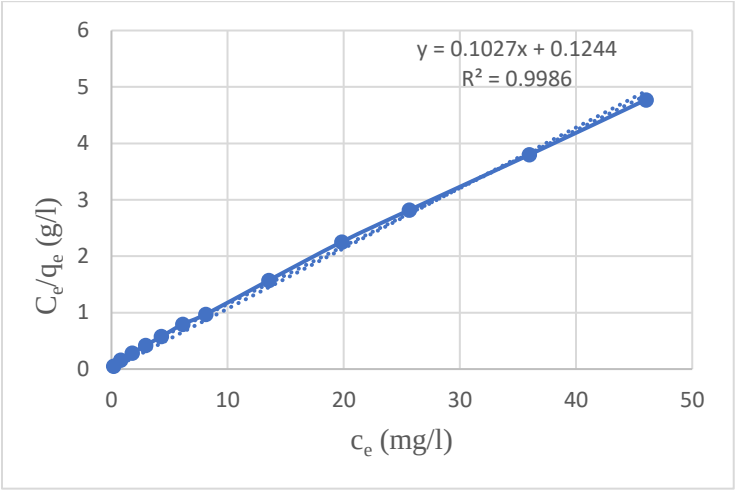

Figure 21: Linearized Langmuir isotherm for Cu^{2+} Ions adsorption onto ARC

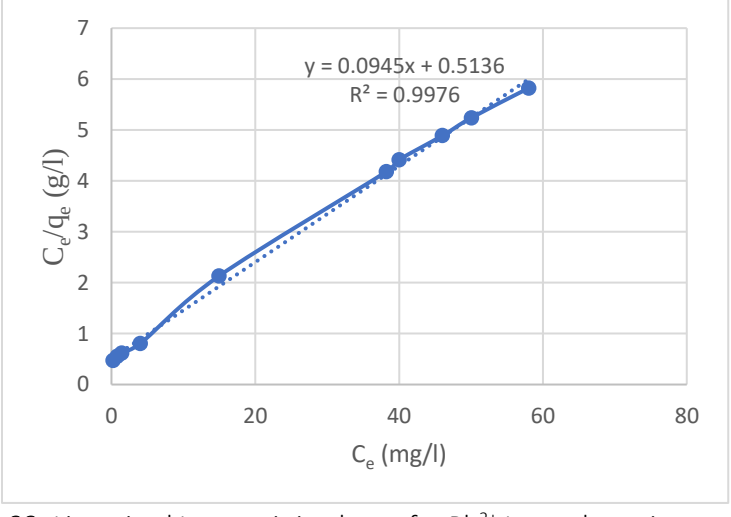

Figure 22: Linearized Langmuir isotherm for Pb^{2+} Ions adsorption onto ARC

From the figures, a straight line where $1/q_{max}$ and K_L were obtained from slope and intercept, respectively. All the K_L values were between 0 and 1, thus favourable reactions. The higher affinity for Cu^{2+} (R^2=0.9986) could be attributed to its smaller hydrated ionic radius (4.19 Å) compared to Pb^{2+} (4.01 Å) and its higher electronegativity, allowing for stronger surface complexation. The same trend was observed in ACC and ACS with KL values between 0 and 1, indicating favourable reactions. The R2 values were 0.9981, 0.9985, 0.9983 and 0.9981 in ACC and 0.9930, 0.9931, 0.9928 and 0.9938 in ACS for Co2+, Cu2+, Pb2+ and RB, respectively. For the Freundlich model, the three metals and the dye gave a good correlation coefficient. Values of regression coefficients, R^2, for Co^{2+}, Cu^{2+}, Pb^{2+} ions and RB were found using the three adsorbents. Adsorption of linearized Freundlich isotherms for adsorption of Co^{2+}, Cu^{2+} and Pb^{2+} ions and RB dye in ARC plotted as log q_e against log C_e are given in **Figures 23** to **25**.

.

Table 4: Langmuir isotherm model parameters for adsorption of Co^{2+}, Cu^{2+}, Pb^{2+} ions and RB dye

		Adsorbates			
Adsorbent	Langmuir isotherm	Co^{2+}	Cu^{2+}	Pb^{2+}	RB
ARC	$q_{max(mg^{-1})}$	0.1009	0.1027	0.0945	0.1146
	$K_{L(Lmg^{-1})}$	0.1399	0.1244	0.5136	0.1423
	R^2	0.9935	0.9986	0.9976	0.9983
ACC	$q_{max(mg^{-1})}$	0.0964	0.0958	0.0959	0.0961
	$K_{L(Lmg^{-1})}$	0.1317	0.1302	0.1307	0.1432
	R^2	0.9989	0.9985	0.9976	0.9981
ACS	$q_{max(mg^{-1})}$	0.1035	0.1024	0.1023	0.1037
	$K_{L(Lmg^{-1})}$	0.1987	0.1994	0.2032	0.1807
	R^2	0.9946	0.993	0.9928	0.9938

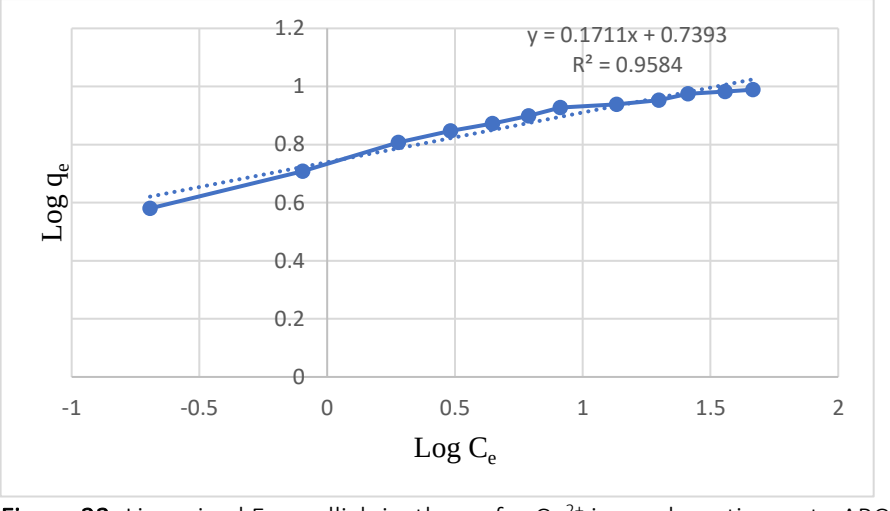

Figure 23: Linearized Freundlich isotherm for Co^{2+} ions adsorption onto ARC

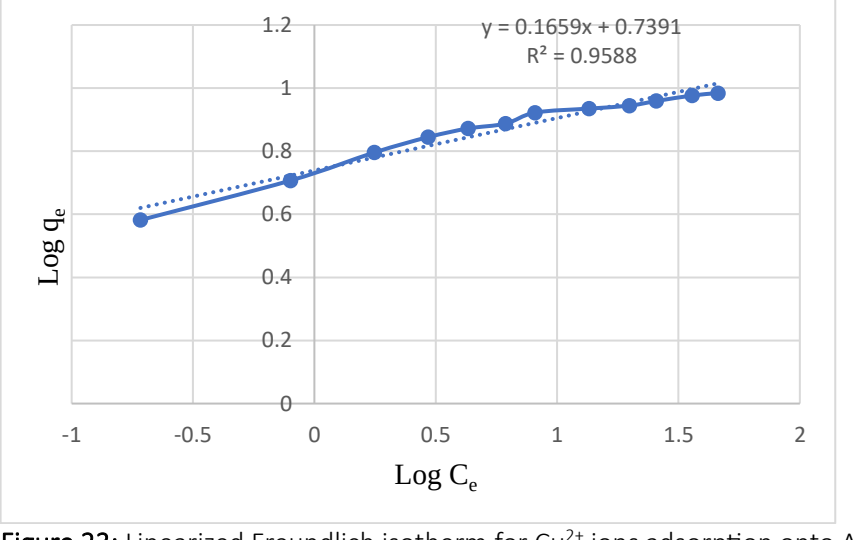

Figure 23: Linearized Freundlich isotherm for Cu^{2+} ions adsorption onto ARC

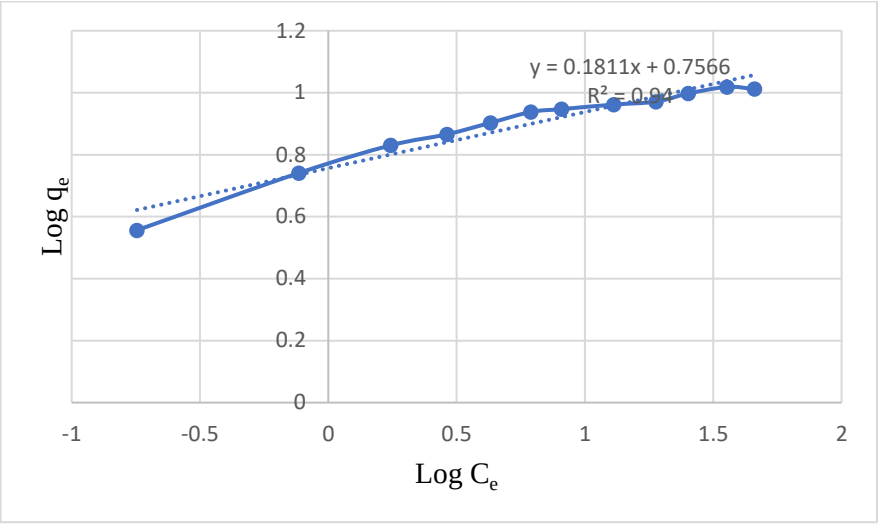

Figure 25: Linearized Freundlich isotherm for Pb^{2+} ions adsorption onto ARC

Compared with Langmuir R^2, Freundlich values were slightly lower as shown in **Table 5.**

Table 5: Freundlich and Langmuir isotherm R^2 for the removal of Co^{2+}, Cu^{2+}, Pb^{2+} ions and RB dye

		Adsorbates			
Isotherm model	Adsorbent	Co^{2+}	Cu^{2+}	Pb^{2+}	RB
Langmuir	ARC	0.9935	0.9986	0.9976	0.9983
	ACC	0.9989	0.9985	0.9976	0.9981
	ACS	0.9946	0.993	0.9928	0.9938
Freundlich	ARC	0.9671	0.9588	0.9424	0.9529
	ACC	0.9729	0.9676	0.94	0.9616
	ACS	0.9319	0.9231	0.9106	0.92

Adsorption Thermodynamics

The nature of the adsorption of Co^{2+} Cu^{2+}, Pb^{2+} ions and RB dye on the prepared adsorbents was predicted by estimating the thermodynamic parameters by varying temperature. The changes in thermodynamic parameters involving free energy (ΔG^o), enthalpy (ΔH^o) and entropy (ΔS^o) were calculated from the following equations.

$$K_e = \frac{q_e}{C_e}$$

$$\Delta G^o = -RT\ln K_e$$

Also,

$$\Delta G° = \Delta H° - T\Delta S°$$

Hence,

$$-RT\ln K_e = \Delta H° - T\Delta S°$$

Rearranging this gives,

$$\ln K_e = \frac{\Delta S^0}{R} + \frac{\Delta H^0}{RT}$$

The equation involves ΔH^o and ΔS^o, which were obtained from the slopes and intercepts of the plots of ln K_e against 1/T shown in **Figures 23** to **25**.

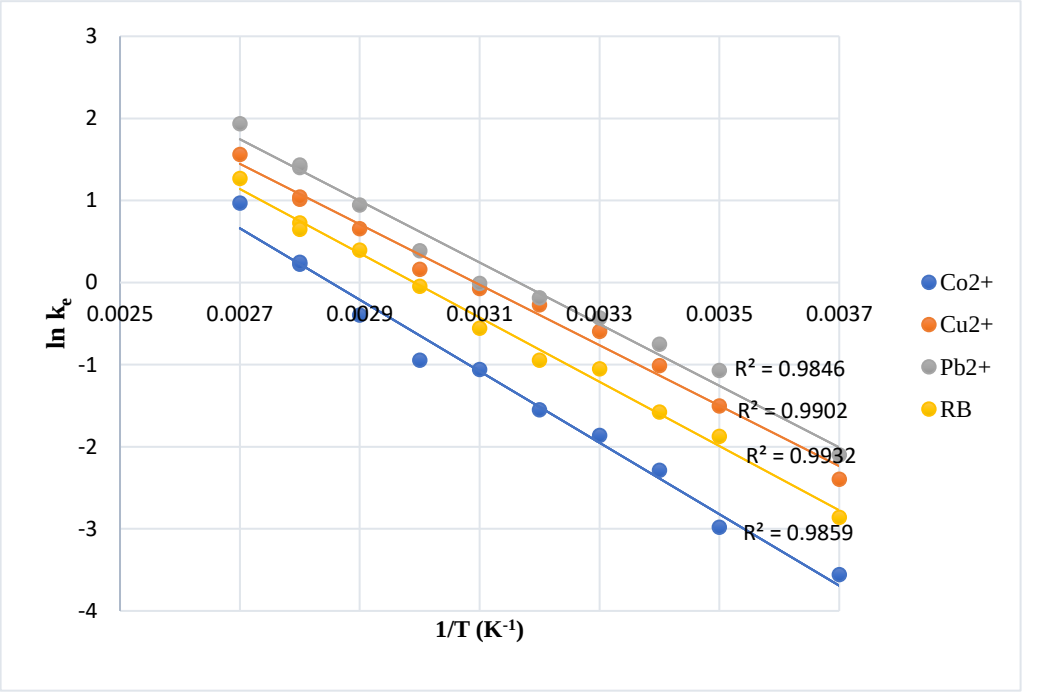

Figure 23: Thermodynamic isotherm for metal ions and dye on ACC

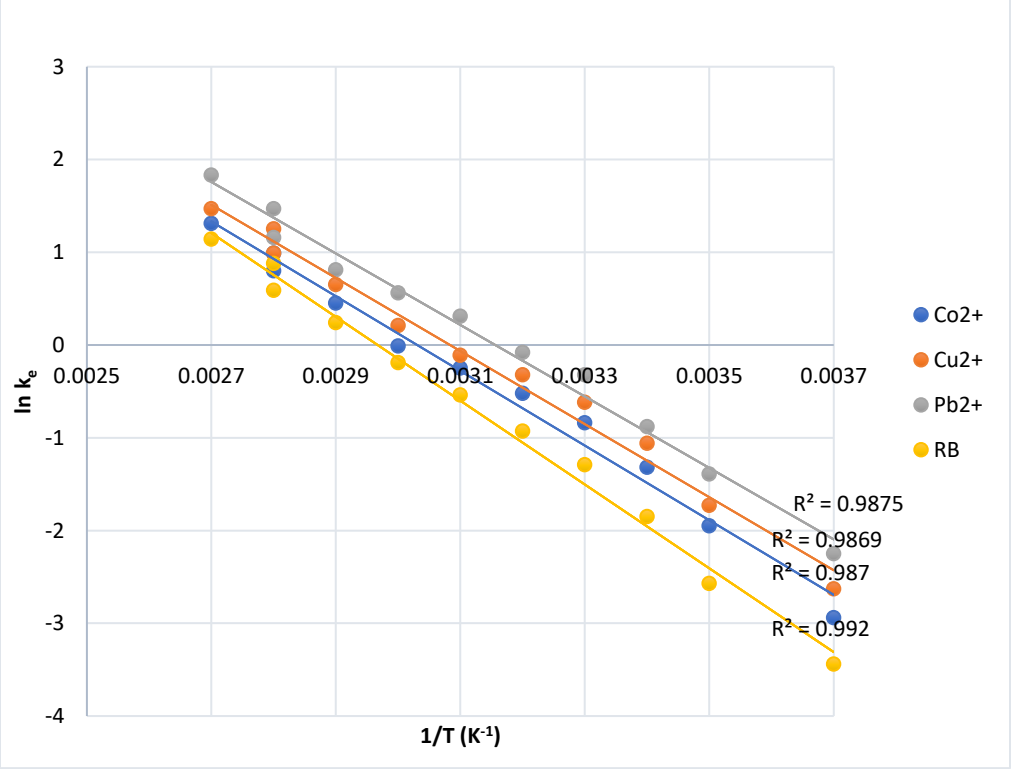

Figure 24: Thermodynamic isotherm for metal ions and dye on ARC

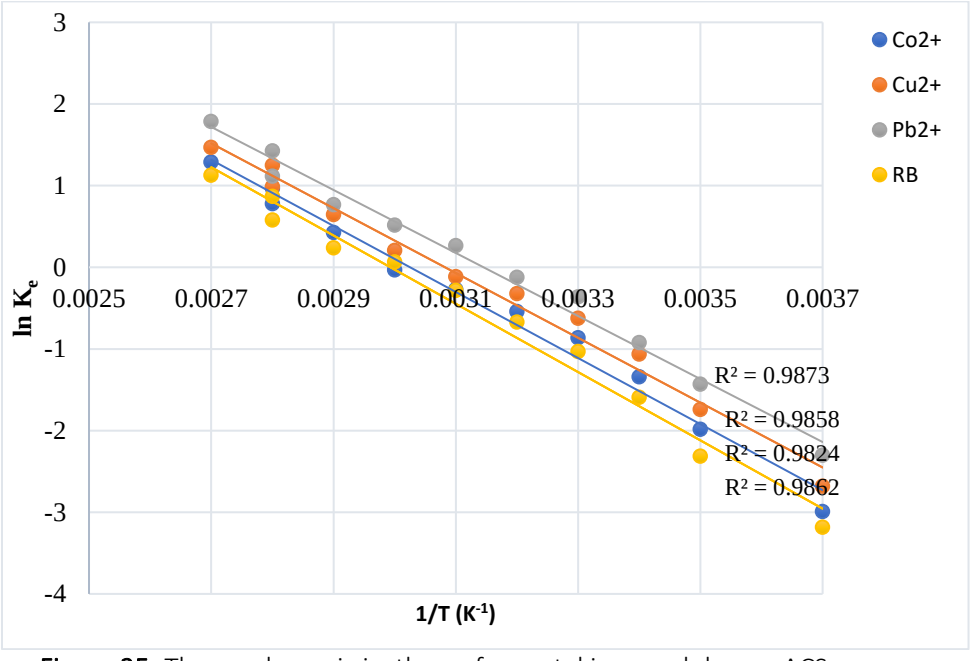

Figure 25: Thermodynamic isotherm for metal ions and dye on ACS

The free energy change (ΔG°) indicates the degree of spontaneity of the adsorption process and the higher negative value reflects a more energetically favourable adsorption. This indicates that the process is entropy driven. Table 6 displays the obtained thermodynamic parameters.

Table 6: Thermodynamic parameters of Co^{2+}, Cu^{2+}, Pb^{2+} and RB adsorption

				ΔG kJ/mol)			
Adsorbent	Adsorbate	ΔH (kJmol^{-1})	ΔS (J/mol/K)	303	313	323	333
ARC	Co^{2+}	33.464	101.36	2.116	1.353	0.671	0.027
	Cu^{2+}	32.745	100.97	1.562	0.832	0.295	-0.581
	Pb^{2+}	32.034	101.11	0.806	0.208	-0.832	-1.55
	RB	37.562	111.45	3.25	2.42	1.45	0.526
ACC	Co^{2+}	36.193	103.218	4.691	3.997	2.817	2.615
	Cu^{2+}	32.54	97.332	1.493	0.6987	0.1885	-0.449
	Pb^{2+}	30.615	94.68	1.083	0.4788	0.0212	-1.074
	RB	31.211	98.787	2.65	2.463	1.488	0.118
ACS	Co^{2+}	33.63	101.738	2.166	1.405	0.725	0.083
	Cu^{2+}	33.002	101.73	1.662	0.833	0.295	0.581
	Pb^{2+}	30.08	111.449	0.907	0.312	-0.725	-1.14
	RB	34.76	104.041	2.594	1.744	0.752	-0.194

At high temperatures such as 333K, negative values imply spontaneity of adsorption. This confirms favourability and spontaneity of adsorption (Ramdani *et al.,* 2020). The adsorption processes were endothermic, the contacts were, however, not spontaneous, and the ΔH values were positive. In the range of 303 to 333 K, non-spontaneity reduced as temperature increased. Therefore, a minor activation energy barrier had to be overcome for the adsorption of Co^{2+}, Cu^{2+}, Pb^{2+} ions, and RB dyes onto ARC, ACC, and ACS. An increase in energy supply made it simpler for them to adsorb onto the adsorbent's surface. There have also been prior reports of such activated adsorption that follows an endothermic course (Futalan *et al*., 2011). The order of ΔH° and ΔS° values was Co^{2+} >RB> Cu^{2+} > Co^{2+}. This is because of strong chemical interactions between Co^{2+} ions and binding sites which require more ΔH^{o} energy and major structural changes of the adsorbent sites (higher values of ΔS^{o}) (Ramdani *et al.,* 2020) and this decreased in that order. Both ΔH^{o} and ΔS^{o} seem to control adsorption using the adsorbents due to high values. The positive ΔS° values reflected affinity of the metal ions onto raw and modified surface sites (Maleki *et al.,* 2015). This confirms the increasing randomness at the solid-solution interface during sorption.

Furthermore, the activation energy (Ea) can be determined from the straight line of $\ln K_e$ against 1/T using the Arrhenius equation:

$$\ln K_e = \ln A - Ea/RT$$

The calculated E_a from the slopes ($-E_a/R$) from these plots were found to be between 3.3×10^{-4} and 3.8×10^{-4} kJ/mol for ARC, 3.1×10^{-4} and 3.6×10^{-4} kJ/mol and 3.2×10^{-4} and 3.5×10^{-4} kJ/mol for AC, indicating chemisorption adsorption (Kralik, 2014). This implies the rate-limiting step could be chemically controlled.

Adsorption Kinetics

Adsorption kinetics and the rate constants can be determined from kinetic models including the pseudo-first order and pseudo-second order models, based on equilibrium adsorption equations below;

$$\ln(q_e - q_t) = \ln q_e - k_1 t \quad \text{and}$$

$$\frac{1}{q_t} = \frac{1}{k_2 q^2_e} + \frac{1}{q_e} t$$

Where q_e and q_t are amounts of metal ions adsorbed onto the adsorbents in mg/g at equilibrium and at a time t, respectively. k_1 and k_2 are rate constants for pseudo-first and second order kinetics, respectively. The first order constant (min^{-1}) can be determined in linear form by plotting q_t against t. Plotting t/q_t against t allows one to calculate pseudo second order (mg/g/min) (Argun *et al.,* 2006). Regarding pseudo first order model, k_1 is low implying a slow adsorption process, while for pseudo second order model, k_2 values were higher indicating an increase in adsorption rates.

The first-order adsorption rate constant, k_1 (min^{-1}), and the pseudo-second-order rate constant, k_2 ($g\ mg^{-1}\ min^{-1}$), were calculated from the intercept of the corresponding plots of t versus q_t and t/q vs. t and are tabulated in **Table 7** along with correlation coefficients, q_e (expected) and q_e (calculated) values. Pseudo first and second thermodynamic kinetic isotherms for metal ions and dye on ARC are shown in **Figures 26** and **27.**

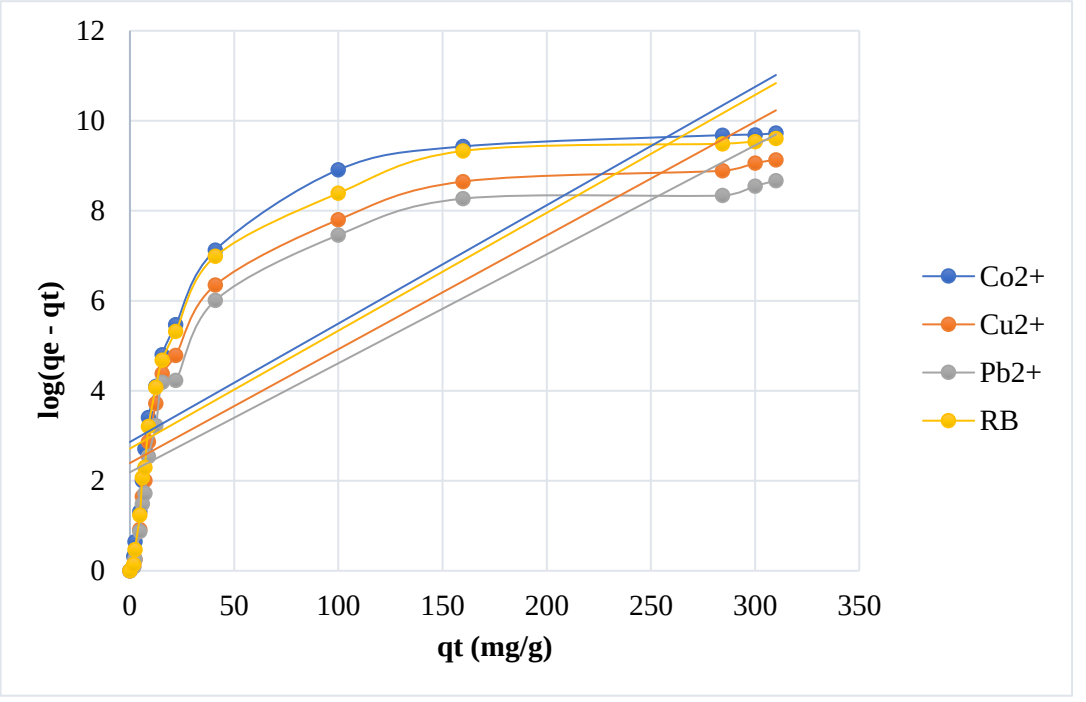

Figure 26: Pseudo first order thermodynamic kinetic isotherm for metal ions and dye on ARC

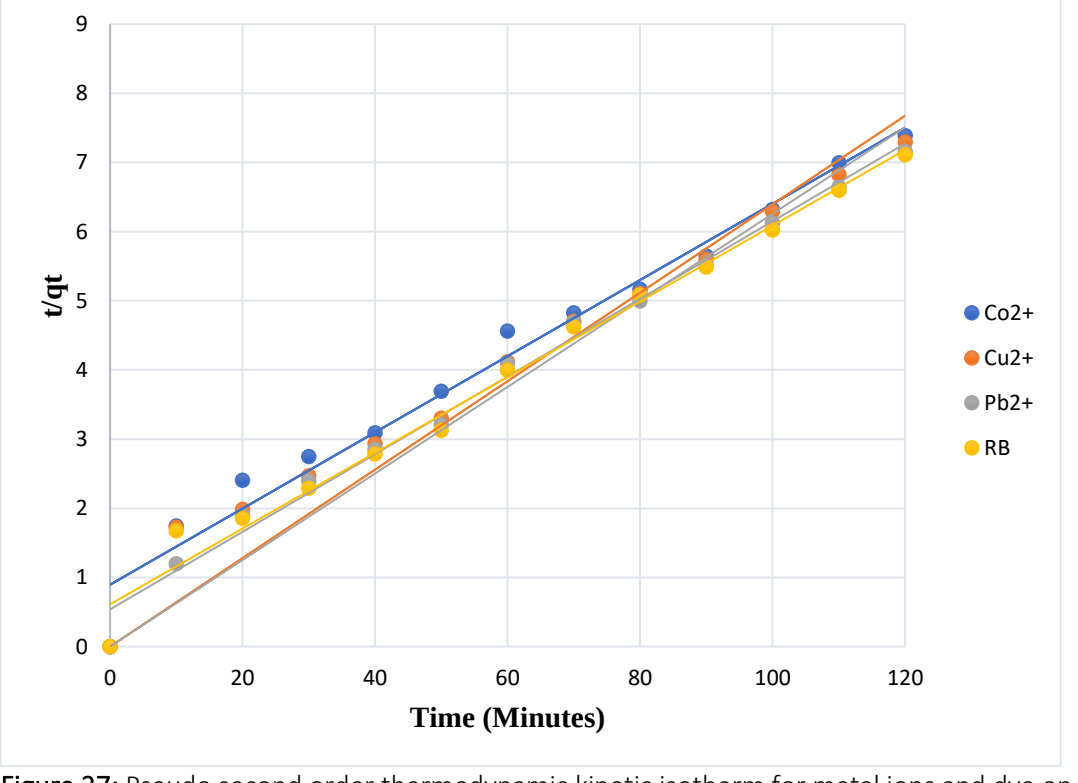

Figure 27: Pseudo second order thermodynamic kinetic isotherm for metal ions and dye on ACC

Table 7: Kinetics parameters for the Co^{2+}, Cu^{2+} and Pb^{2+} ions ad RB dye adsorption

		Pseudo-first order				Pseudo-second order		
Adsorbent	Adsorbate	$q_{e(exp)}$ (mg/g)	$q_{e(cal)}$ (mg/g)	K_1 (mg/g/min)	R^2	$q_{e(cal)}$ (mg/g)	K_2 (mg/g/min)	R^2
ARC	Co^{2+}	2.5	0.3494	2.862	0.6942	1.1181	0.8937	0.9761
	Cu^{2+}		0.4177	2.3985	0.702	1.563	0.6274	0.9568
	Pb^{2+}		0.4567	2.1901	0.7245	1.597	0.1196	0.9728
	RB		0.3684	2.7144	0.7185	1.6353	0.6085	0.986
ACC	Co^{2+}	2.5	0.3854	2.5947	0.07052	1.1063	0.8979	0.9762
	Cu^{2+}		0.473	2.1142	0.7284	1.5119	0.6631	0.9861
	Pb^{2+}		0.5547	1.8028	0.7072	2.006	0.4965	0.992
	RB		0.4173	2.3964	0.7141	1.7608	0.5685	0.9873
ACS	Co^{2+}	2.5	0.408	2.451	0.7277	1.1091	0.9002	0.9761
	Cu^{2+}		0.4952	2.0194	0.7439	1.5312	0.6541	0.9855
	Pb^{2+}		0.5756	1.7373	0.7667	1.9029	0.5271	0.991
	RB		0.4305	2.3229	0.7097	1.5903	0.629	0.984

The kinetic models were evaluated for conformance, application, and acceptability using the correlation coefficient (R^2). The coefficients for the pseudo-second order were higher than for the pseudo-first order. The adsorption of dye and metal ions on ARC, ACC, and ACS is best represented by the pseudo second order mechanism, indicating the rate-limiting step is a chemical adsorption. The R^2 values for pseudo-second order in all the three adsorbents studied are above 0.95, which is near to 1 (Al-Ghouti and Da'ana, 2020).

Conclusion

The study's findings indicate that ARC, ACC, and ACS can be used as safe, natural, economical, and environmentally acceptable adsorbents to remove ions such as Co^{2+}, Pb^{2+}, Cu^{2+}, and RB dye from aqueous solutions. The surface area, phase identification, and functional groups responsible for eliminating dye and metal ions from aqueous solutions were examined using BET, XRD, and FTIR. The batch adsorption process was influenced by temperature, pH of the solution, size, dosage, and contact duration. Natural adsorbents such as clay soil, coconut shells, and easily accessible rice husks could be used because of their high removal efficiencies of the metal ions and dye used in this work. The process followed the Langmuir isotherm and Pseudo-second order kinetics, as this confirms the nature of the adsorption (monolayer chemisorption). ARC proved

to be the best followed by ACC and ACS in this order. From the free energy change (ΔG^{o}), the degree of spontaneity of the adsorption process and the higher negative value reflects a more energetically favourable adsorption and the process was entropy driven.

Recommendations

The facts and conclusions described above point to the need for more study on the following subjects:

i. Researching the efficacy of ARC, ACC, and ACS in eliminating various contaminants, including pesticides, other inorganic pollutants, organic pollutants, and pharmaceutical waste effluents, is crucial.
ii. The study's biosorbents must be tested to determine whether they can extract heavy metal ions from real water samples.
iii. A comparison study of the effectiveness and efficiency of clay, coconut shells, rice husk, and other biomass should be carried out using different ratios.
iv. Research on adsorbents to see if they can be recycled with the right regenerating agent to save costs.
v. Investigating surface modification or chemical activation methods to enhance the adsorption capacity, selectivity, and stability of ARC, ACC, and ACS toward specific pollutants.
vi. Scaling up from laboratory batch studies to continuous-flow column experiments to evaluate the suitability of the adsorbents for industrial and municipal water treatment applications.
vii. Performing economic feasibility and life-cycle assessments to determine the cost-effectiveness, environmental impact, and commercial viability of producing and using these biosorbents on a large scale.
viii. Examining the potential recovery of adsorbed heavy metals from spent adsorbents for resource recovery and safe disposal, thereby supporting circular economy approaches in wastewater treatment.
ix. Exploration of hybrid treatment systems combining adsorption with other techniques (e.g., membrane filtration, photocatalysis, coagulation).

References

Al-Ghouti, M. A. and Da'ana, D. A. (2020). Guidelines for the use and interpretation of adsorption isotherm models. *A review, Journal of Hazardous Materials*, **393**: 122-383. https://www.sciencedirect.com/science/article/pii/S030438942030371X

Argun, M. E., Dursun, S., Ozdemir, C., and Karatas, M. (2006). Heavy metal adsorption by modified oak sawdust: Thermodynamics and kinetics. *Journal of Hazardous Materials*, **141**, 77–85. https://doi.org/10.1016/j.jhazmat.2006.06.095

Bakti, A. I. and Gareso, P. L. (2018). Characterization of Active Carbon Prepared from Coconuts Shells Using FTIR, XRD and SEM Techniques. *Jurnal ilmiah pendidikan fsika Al-Biruni* **7**:33-39. https://ejournal.radenintan.ac.id/index.php/al-biruni/article/view/2459

Banerjee, S., Aditya, G. and Saha, G. K. (2016). Household disposables as breeding habitats of dengue vectors: Linking wastes and public health. *Elsevier*; **33**(1): 233-239. https://doi.org/10.1016/j.wasman.2012.09.013

Chengo, K., Murungi, J. and Mbuvi, H. (2013). Speciation of Zinc and Copper in Open-Air Automobile Mechanic Workshop Soils in Ngara Area-Nairobi Kenya. *Resources and Environment*, **3:** 145-154. https://ir-library.ku.ac.ke/items/59dd3613-b9b7-4745-a2c5-9926ba1ccc62

Futalan, C. M., Kan, C. C., Dalida, M. L., Hsien, K. J., Pascua, C. and Wan, M. W. (2011). Comparative and competitive adsorption of copper, lead and nickel using chitosan immobilized on bentonite. Carbohyd. Polym., **83**, 528-536. https://doi.org/10.1016/j.carbpol.2010.08.013

Hawali, H., Matin, A. and Suherman, S. (2023). Rice husk waste: Impact on environmental health and potential as biogas. Sispae; **18**(3): 431-436. https://journal.unnes.ac.id/nju/kemas/article/view/42467

Hegazi, H. A. (2013). Removal of heavy metals from wastewater using agricultural and industrial wastes as adsorbents. *HBRC Journal* ***9***(3), 276-282. https://doi.org/10.1016/j.hbrcj.2013.08.004

Irannajad, M. and Haghighi, H. K. (2017). Removal of Co2+, Ni2+ and Pb2+ by manganese oxide-coated eolite: Thermodynamics and kinetic studies. Clays and clay minerals. **65**: 52-62. https://www.cambridge.org/core/journals/clays-and-clay-minerals/article/abs/removal-of-co2-ni2-and-pb2-by-manganese-oxidecoated-zeolite-equilibrium-thermodynamics-and-kinetics-studies/C27423F17872D43F833414894400F667

Kant, R. (2012). Textile dyeing industry an environmental hazard. *Natural science,* **4**:22-26. https://pdfs.semanticscholar.org/0807/fade7c6c26e2195dc7c5f37e806128a8e73a.pdf

Khan, A., Naqvi, H. J., Afzal, S., and Jabeen, S. (2017). Efficiency Enhancement of Banana Peel for Wastewater Treatment through Chemical Adsorption. *Academy of Sciences: A. Physical and Computational Sciences*, **54**(3), 329–335.

Kralik, M. (2014). Adsorption, Chemisorption and Catalysis. Chemical Paper, **68**(12): 1625 – 1638. https://doi.org/10.2478/s11696-014-0624-9

Kudesia, V. P. (2000). Environmental Chemistry. *Pragati Prakasan Merrut,* 114-150.

Levin, R., Brown, M. J., Kashtock, M. E., Jacobs, D. E., Whelan, E. A., Rodman, J., and Sinks, T. (2008). Lead exposures in US children, 2008: implications for prevention. *Environmental Health Perspectives*, **116:** 1285. https://pmc.ncbi.nlm.nih.gov/articles/PMC2569084/

Maleki, A., Pajootan, E. and Hayati, B. (2015). Ethyl acrylate grafted chitosan for heavy metal removal from wastewater: Equilibrium, kinetic and thermodynamic studies. *Journal of the Taiwan Institute of Chemical Engineers*, **51**: 127–134. https://doi.org/10.1016/j.jtice.2015.01.004

Manyangadze, M., Chikuruwo, N. M. H., Narsaiah, T. B., Chakra, C. S., Charis, G., Danha, G., and Tirivaviri, A. M. (2020). Adsorption of lead ions from wastewater using nano silica spheres synthesized on calcium carbonate templates. *Heliyon*, **6**(11): 1–13. https://www.cell.com/heliyon/fulltext/S2405-8440(20)32152-6

Mataka, L., Salidu, S., Masamba, W. and Mwatseteza, J. (2010). Cadmium sorption by *Moringa stenopetala* and *Moringa oleifera* seed powder. *International Journal Environmental Science Technology*, **3:** 131-139. https://academicjournals.org/journal/IJWREE/article-full-text-pdf/B8699CB1648

Naja, G. M., Mustin, C., Volesky, B., and Betherlin, J. (2010). Biosorption study in a mining wastewater reservoir. *Int. J. Environ. Pollut*., **34** (1-4): 14 – 27. https://www.inderscienceonline.com/doi/abs/10.1504/IJEP.2008.020779

Nakbanpote, W., Goodman, B. A. and Thiravetyan, P. (2007). Cooper adsorption on rice husk derived materials studied by EPR and FTIR. Colloid, Surface, A, **304**: 7-13. https://doi.org/10.1016/j.colsurfa.2007.04.013

Pang, T., Yang Z., Huang, Y., Lei, X., Zeng, X., Li, X. (2018). Adsorption Properties of Thiol-Modified, Sodium-Modified and Acidified Bentonite for Cu^{2+}, Pb^{2+} and Zn^{2+} *Spectrosc. Spectr. Anal.* **38**:1203–1208.

Ramdani, A., Kadechea, A., Adjdirb, M., Taleb, Z., Ikhoua, D., Taleb, S. and Deratani, A. (2020). Lead and cadmium removal by adsorption process using hydroxyapatite porous materials. *Water Practice and Technology*, **15** (1): 130–141. https://iwaponline.com/wpt/article-abstract/15/1/130/71825/Lead-and-cadmium-removal-by-adsorption-process

Salleh, M. A. M., Mahmoud, D.K., Karim, W.A. and Idris, A. (2011). "Cationic and anionic dye adsorption by agricultural solid wastes: a comprehensive review". Desalination **280**(1-3), 1-13. https://doi.org/10.1016/j.desal.2011.07.019

Singh, D. K., Srivastave, B. and Bharadwas, R. K. (2001). Removal of Chromium (VI), Iron (II) and Mercury (II) from Aqueous Solutions using Activated Carbon Obtained from Tea Leaves. *Pollution Resources* **20** (2); 173-177.

Srivastava, V., Shekhar, M., Gusain, D., Gode, F., and Sharma, Y. C. (2017). Application of a heterogeneous adsorbent (HA) for the removal of hexavalent chromium from aqueous solutions: Kinetic and equilibrium modeling. *Arabian Journal of Chemistry*, **10**: 1– 26.

Tayeh, B. A., Alyousef, R., Alabduljabbar, H. and Alaskar, A. (2021). Recycling of rice husk waste for a sustainable concrete: A critical review. *Elsevier*; 312. https://www.sciencedirect.com/science/article/abs/pii/S0959652621019521

Tong, S., Schirnding, Y., Von, E. and Prapamontol, T. (2000). Environmental lead exposure: a public health problem of global dimensions. *Bulletin of the World Health Organization*, **9:** 1068-1077. https://www.cabidigitallibrary.org/doi/full/10.5555/20002017024

Vieira, M. G. A., De-Almeida, N. A. F., Da-Silva, M. G. C., Carneiro, C. N. and Melo, F. A. A. (2013). Adsorption of Lead and Copper Ions from Aqueous Effluents on Rice Husk Ash in a Dynamic System. *Brazilian Journal of Chemical Engineering,* **31**(2):519 – 529. https://doi.org/10.1590/0104-6632.20140312s00002103

Wang, X. S. Huang, J. H., Wang, J. and Qin, Y. (2007). Determination of kinetic and equilibrium parameters of the batch adsorption of Ni(II) from aqueous solutions by Na-mordenite. *J. Hazard. Mater.* **142:** 468-476. https://doi.org/10.1016/j.jhazmat.2006.08.047

Zhao, H. and Lang, Y. (2018). Adsorption behaviors and mechanisms of florfenicol by magnetic functionalized biochar and reed biochar. *Journal of the Taiwan Institute of Chemical Engineers*, **88**: 152-160. https://doi.org/10.1016/j.jtice.2018.03.049

Zhao, M., Wang, S., Li, Y., Wang, H., Qin, P., Kong, F. (2019). Competitive adsorption of Cu^{2+}, Pb^{2+}, Zn^{2+} and Cd^{2+} by new-sodium titanate filler. *Acta Sci. Circ.* **39**:390–398.